 FDMP, vol.6, no.1, pp.109-136, 2010

Effect of Confined and Heated Ambient Air on Onset of Instability in Liquid Bridges of High Pr Fluids

Shaligram Tiwari[1] **and Koichi Nishino**[2]

Abstract: The present work reports about an experimental study investigating the influence of air convection and of ambient temperature around a half-floating zone on the transition behavior from steady to oscillatory flow, i.e. the influence on the critical Marangoni number (Ma_{cr}). Increase of heat loss from the free surface of the half-floating zone or liquid bridge by increased convection and ambient cooling decreases Ma_{cr}. Heat input to the free surface increases Ma_{cr}. An add-on numerical simulation of the air convection around the zone clarifies the influence of air convection and the ambient temperature on the temperature, surface velocity and local Biot number at the free liquid surface.

Keywords: Thermocapillary convection, liquid bridge, heated ambient air, onset of oscillatory instability, interfacial heat transfer

1 Introduction

A temperature gradient at the interface between two immiscible liquids or between a liquid and a gas generates a surface tension gradient and hence a bulk fluid motion through viscous diffusion. Thermocapillary convection (TC) can be found as an important or even dominant effect in various small scale systems and most prominently under microgravity environments as discussed by Ostrach (1979) in his studies on low gravity fluid flows. The investigations to explore this phenomenon are very useful especially for studies involving crystal growth phenomena for high quality material processing. The most common configuration for simulation of thermocapillary flows is that of a half-floating-zone or liquid bridge, in which a liquid column is suspended between two differentially heated walls. In general, crystal melts have low *Pr* due to which studies with high *Pr* fluids do not actually

[1] Department of Mechanical Engineering, Indian Institute of Technology Madras, Chennai-600036, India, Email: shaligt@iitm.ac.in

[2] Department of Mechanical Engineering, Yokohama National University, 79-5, Tokiwadai, Hodogaya-ku, Yokohama-2408501, Japan, Email: nish@ynu.ac.jp

simulate the float zone. Nevertheless, tests with high *Pr* fluids are interesting because it is found that the flow becomes oscillatory beyond certain value of temperature difference across the liquid bridge. The oscillation phenomenon for the liquid bridge was first reported by Chun and Wuest (1979) and Schwabe, Scharmann, Preisser and Oeder (1978). However, the mechanism and causes of flow becoming oscillatory are always open to investigations. Kuhlmann and Rath (1993) and Masud, Kamotani. and Ostrach (1997) investigated instabilities in cylindrical liquid bridges. The other experimental studies of transition from steady to oscillatory thermocapillary flows were carried out by Chun (1980) and Schwabe, Scharmann and Preisser (1981). The behavior of oscillation of the liquid bridge was analytically studied by Pimputkar and Ostrach (1980) and Kamotani and Ostrach (1998). Smith and Davis (1983) studied the convective instabilities of dynamic thermocapillary liquid layers with side heating for fluids of different *Pr* values and observed that for high *Pr* fluids the dominant mechanism of instability appears in the form of longitudinal rolls and critical Marangoni number (Ma_{cr}) for conducting interfaces is higher than that for an insulated interface.

The stability and shape of liquid bridges are strongly influenced by gravity as well as the surface tension and nature of liquid support contact. A liquid that is stable in zero gravity (microgravity) would deform and may collapse under earth's gravity. This is because the buoyancy effect is significant in ground-based experiments. Oscillatory buoyant thermocapillary flow in cylindrical liquid bridges was experimentally investigated under microgravity by Monti, Albanese, Cartenuto, Castagnolo and Evangelista (1995). Recently, Wang, Kamotani and Yoda (2007) reported from a combined experimental and numerical study on oscillatory thermocapillary flow in liquid bridges of high Pr fluid. They emphasized that compared to an insulated surface of a liquid bridge, even the condition of heat gain can trigger the onset of instability in convex liquid bridges ($\mathrm{D/D_0} < 0.8$) due to interaction between buoyancy and thermocapillarity. The interaction between thermocapillarity and buoyancy is less prominent for concave liquid bridges.

Kobayashi (1984) studied numerically the steady flow in a cylindrical floating zone under low gravity. Wanschura, Shevtsova, Kuhlmann and Rath (1995) investigated numerically the mechanisms of convective instabilities in thermocapillary liquid bridges. Shevtsova, Melnikov and Legros (2001) carried out three-dimensional simulations of hydrodynamic instability in liquid bridges by considering the influence of temperature dependent viscosity. Lai (2004), in his numerical study, carried out multiple-scale analysis of oscillatory TC of high *Pr* fluids in a rectangular cavity. Leypoldt, Kuhlmann and Rath (2000) conducted three-dimensional numerical study on TC flows in cylindrical liquid bridges. Imaishi, Yasuhiro, Akiyama and Yoda (2001) carried out numerical simulation of oscillatory TC in half-zone of low

Pr fluid. Gelfgat, Rubinov, Bar-Yoseph and Solan (2005) investigated numerically the three-dimensional instability of TC in cylindrical undeformable floating zones heated laterally. An important result from their study is in the form of stability diagrams which show the Prandtl number dependence of the critical Marangoni numbers that represent the thermocapillary forcing for different heating conditions.

For a half-zone confined between two differentially heated rods/ rods, an increase of Marangoni number (Ma) beyond its critical value (Ma_{cr}) causes onset of an oscillatory flow. Shevtsova, Melnikov and Legros (2004) studied numerically the changes of flow patterns in TC of liquid bridges. They studied spatio-temporal patterns of thermocapillary flow from onset of instability up to the appearance of the non-periodic flow. Ueno, Tanaka and Kawamura (2003) studied oscillatory and chaotic TC in a half-zone liquid bridge experimentally. They categorized the induced thermocapillary flows in liquid bridges into several regimes mainly by using the patterns of the suspended particle motion in the bridge and the surface temperature variation. Their observation revealed that during the transition, the nature of the flow changed first to chaotic and then to turbulent.

Onset of the oscillatory TC in a half-zone is known to be sensitive to heat transfer at the free surface of the liquid bridge and the ambient air motion. Velten, Schwabe and Scharmann (1991) described the effect of heat loss from the free surface of a liquid bridge under various conditions of heating from top and from below. Kamotani, Wang, Hatta, Wang and Yoda (2003) have shown that onset of instability is very sensitive to heat transfer across the free surface of the liquid bridge, such that the critical temperature (ΔT_{cr}) may change by two to three times when the ambient temperature is varied. Shevtsova, Mialdun and Mohamed (2005) studied the heat transfer behavior in liquid bridges near onset of instability. In order to realize various heat transfer possibilities, they conducted experiments in open air environment and in shielded liquid bridges of 5 to 10cSt silicone oil. The aspect ratio (AR) considered by them was more than 1 (AR = 1.2). Kamotani, Wang, Hatta, Wang and Yoda (2003) explained the mechanism of pre-onset (instability appearing at lower value of Ma_{cr}) of instability triggered by heat loss from the free surface. In fact, heat loss enhances the dynamic free surface deformation and makes it easier for the flow to become oscillatory. They employed for the first time insulated partition boundaries in the air surrounding the liquid bridge to control the heat loss from the free surface. Nishino and Tiwari (2007) studied numerically the effect of heat loss on Marangoni convection in a liquid bridge of high Prandtl number fluid for Ma = 13200. In another numerical study over a wide range of Marangoni numbers, Tiwari and Nishino (2007) reported that the effect of increasing ambient temperature on free surface heat transfer in presence of a partition boundary under normal gravity closely mimics the situation under microgravity. The present study attempts

to relate the effect of surface heat loss on the onset of oscillatory instability. The experimental investigations are carried out to find the effect of ambient heating and confined air convection on the onset of instability. The additional part of the present work has been presented as a numerical study to find the effect of ambient temperature on free surface heat loss, free surface temperature and free surface velocity of the liquid bridge over wider ranges of ambient temperature values than were reported by Tiwari and Nishino (2007). The aim of this overall investigation is to relate the effect of free surface heat loss or heat gain on the value of Ma_{cr}.

2 Problem statement

2.1 Description of experimental set up

Figure 1(a) shows the photograph of a liquid bridge of 5cSt silicone oil suspended between two differentially heated rods. The upper heated rod is made of sapphire and the lower cooled rod is made of aluminum. The material of upper rod has been chosen as sapphire mainly because sapphire has good thermal conductivity and offers the benefit of flow visualization in the liquid bridge with the help of a CCD camera mounted on top of the rod. Fig. 1(b) shows the photograph of the complete experimental set up with locations of the CCD camera and the temperature sensor. The photograph in Fig. 1(c) gives a closer view of the partition boundaries (PBs) in the form of annular circular rods mounted coaxially above and below the liquid bridge. The PBs are made of thermally insulating Perspex material. In the present study, the height of liquid bridge has been chosen as L = 2.5mm and its diameter as D = 5mm. The ratio of volume of liquid suspended between the rods to the volume of the actual cylindrical space available between them is called 'volume ratio' (VR). In the present study, four values of VR have been considered, viz. VR = 0.8, 0.9, 1.0 and 1.1. In each case of the study required to find the effect of other parameters on onset of oscillations in the liquid bridge, a new liquid bridge is formed without changing the adjusted separation between the rods. Thus, the height to diameter ratio of the liquid bridge, called 'aspect ratio' (AR), remains fixed as AR = 0.5 while other parameters like VR and ambient air temperature are varied.

In Fig.1(b), two CCD cameras have been mounted, with one kept on top of the sapphire rod and the other placed horizontally in the level of the liquid bridge and it presents a view of flow behavior of the liquid bridge on a LCD screen. The sapphire rod is heated and the aluminum rod is cooled with the help of heating and cooling elements attached to them. The extent of heating and cooling can be used to vary the temperature difference between the rods. The temperatures of the rods are varied in such a way that the mean temperature of the rods (also being assumed as mean fluid temperature) varies very little. This is mainly because in the numerical

study, while considering variation of the Marangoni number, the temperatures of the two rods are varied in such a way that the mean fluid temperature is maintained constant. A temperature sensor records the temperature signal at the surface of the liquid bridge. With increase in the temperature difference between the two rods, the change in flow behavior at liquid-air interface influences the convection characteristics in the surrounding air. The temporal evolution of the air temperature recorded by the sensor near the surface of the liquid bridge is a good indicator of nature of flow in the liquid bridge. In other words, as the surface flow becomes unsteady on the onset of an oscillatory instability, the air temperature close to the interface also fluctuates synchronously. Consequently, as the temperature difference between the two rods reaches a critical temperature difference, the onset of oscillation in the steady convection of liquid bridge observed on the screen can be directly related to a similar change in the nature of temperature signal. Thus, the time history of the temperature signal can be used to find the time instant and the critical temperature difference (ΔT_{cr}) between the two rods when the nature of thermocapillary flow inside the liquid bridge changes from steady to oscillatory. Fig.1(c) shows the mounting of insulating partition boundaries coaxially and symmetrically with respect to the liquid bridge.

2.2 Description of computational domain

Figure 2 shows an axisymmetric computational domain of the cylindrical-shaped liquid bridge of 5cSt silicone oil as considered in the above experimental set up. The diameter, D (=5.0mm) and height, L (=2.5mm) of the liquid bridge are kept same as in the experimental set up. The aspect ratio (AR) of the liquid bridge is 0.5 thereby the height to width ratio of the liquid region in the computational domain becomes 1.0. However, the volume ratio, V/V_0= 1.00 in the considered computational domain because of assuming a plane interface and cylindrical shape of the liquid bridge. Computations are carried out both in absence and presence of partition boundaries so that the role of partition boundary from computed results and experimental results can be related. The annular partition rods serving as partition boundaries have inside diameter equal to 5mm and outside diameter equal to 17.5mm and they are assumed to be thermally insulating. Thus, the axisymmetric computational domain has been chosen to be R = 17.5mm horizontally; $L + 2H$ = 26.5mm vertically in absence of partition rods and $L+ 2H_p$ = 5.0mm vertically in presence of partition rods. This means the partition rods are mounted at H_p = 1.25mm away from upper and lower surfaces of the liquid bridge respectively.

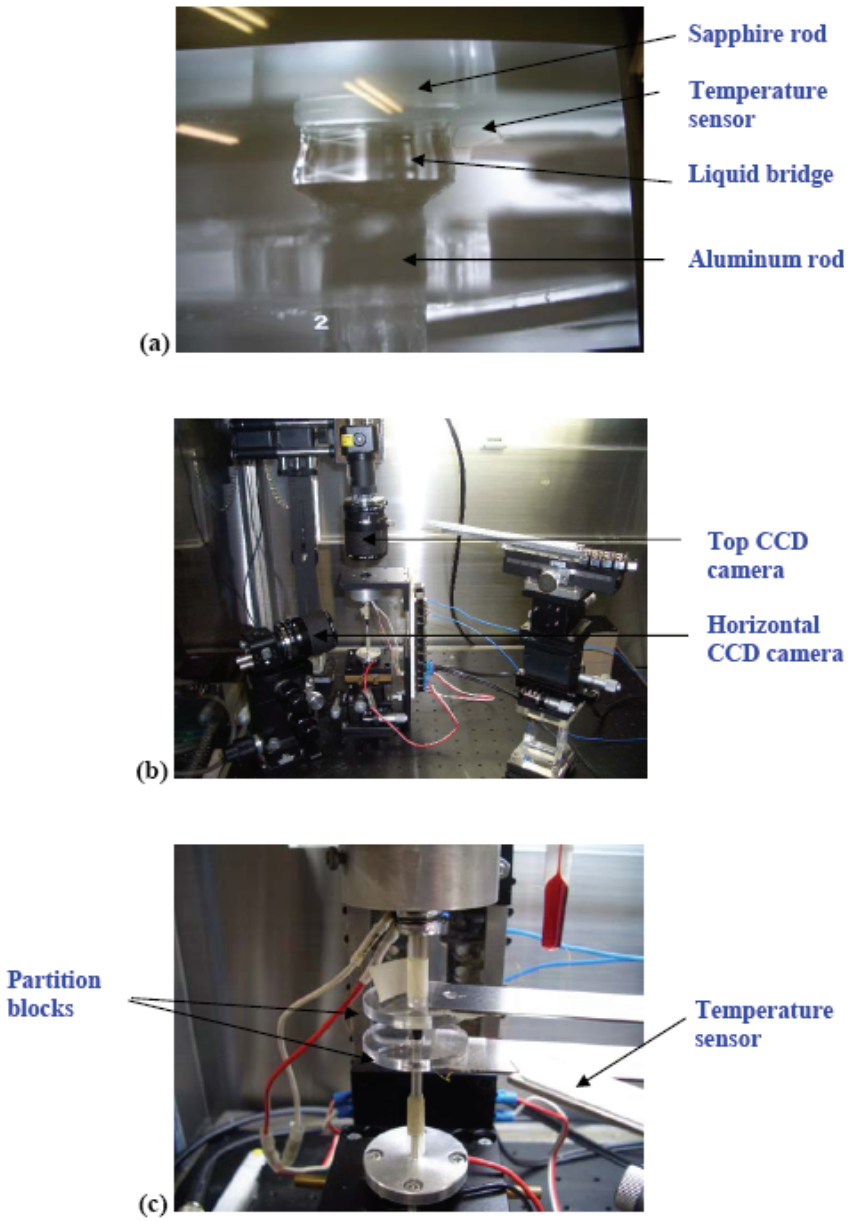

Figure 1: Photographs showing (a) liquid bridge with the temperature sensor (b) the experimental set up with CCD camera and thermocouples (c) partition blocks mounted coaxially with the rods above and below the liquid bridge

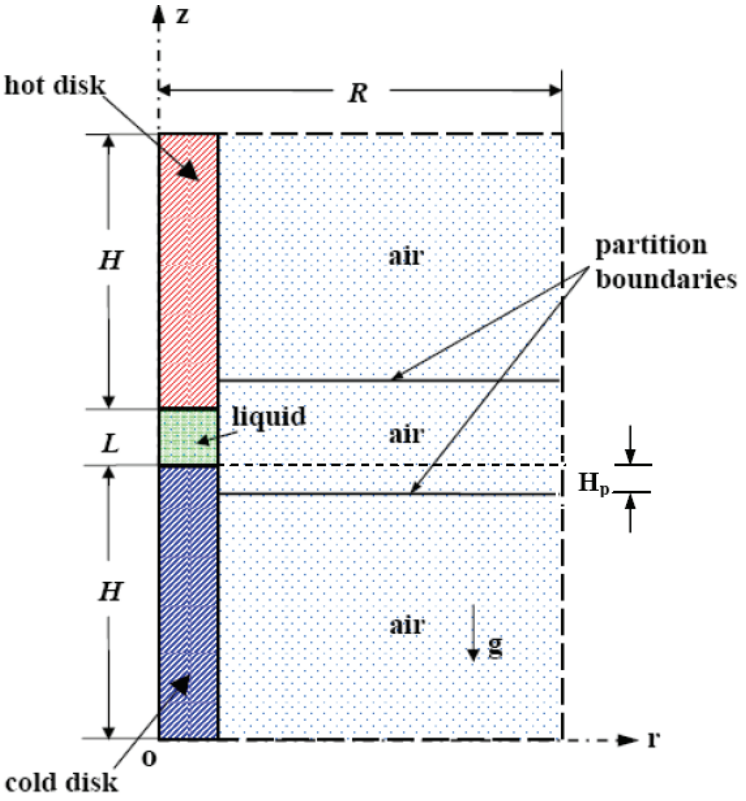

Figure 2: Axisymmetric computational domain showing liquid and air region

3 Basic theory and governing equations

3.1 Basic theory

The behavior of the flow induced by thermocapillary effect can be described by using two non-dimensional numbers, the Marangoni number, Ma, and Prandtl number, Pr, defined as follows.

$$Ma = \frac{\sigma_T \, \Delta T \, L}{\rho \, \nu \, \alpha}, \quad \Pr = \frac{\nu}{\alpha} \tag{1}$$

We can write, Marangoni number as product of Reynolds number and Prandtl number, $Ma = Re_\sigma$ Pr, where $Re_\sigma$is the Reynolds number based on a reference velocity, called Marangoni velocity (u_{ref}). The Reynolds number and the Marangoni veloc-

ity may be written as

$$Re = \frac{\sigma_T \Delta T L}{\rho \nu^2}; \quad \mathrm{u}_{ref} = \frac{\sigma_T \Delta T}{\rho \nu} \tag{2}$$

Here ΔT is the temperature difference between the rods (K or °C), σ_T ($=|\partial\sigma/\partial T|$) is the temperature coefficient of the surface tension, L is the height of the liquid bridge, ρ is the density, ν is the kinematic viscosity and α is the thermal diffusivity of the liquid. The temperature dependence of fluid viscosity cannot be neglected for experiments involving large values of ΔT. The fluid viscosity is calculated at an average temperature $T = (T_H + T_L)/2$ with the use of an empirical correlation given in Ref [19]. If temperature in °C is denoted by 't', then

$$\frac{\nu(t)}{\nu_0} = \exp\left(5.892 \frac{25 - t}{273.15 + t}\right) \tag{3}$$

where ν_0 is the kinematic viscosity at 25 °C.

3.2 Governing equations

The basic governing equations of mass, momentum and energy in their non-dimensional form are given as

$$\nabla . \vec{u}^{(i)} = 0 \tag{4}$$

$$\vec{u}^{(i)} \cdot \nabla \vec{u}^{(i)} = -\nabla p^{(i)} + \frac{1}{Re^{(i)}} \nabla^2 \vec{u}^{(i)} + \frac{Gr^{(i)}}{{Re^{(i)}}^2} T^{(i)} \vec{e}_z + \vec{S} \tag{5}$$

$$\vec{u}^{(i)} . \nabla T^{(i)} = \frac{1}{Re^{(i)} \mathrm{Pr}^{(i)}} \nabla^2 T^{(i)} \tag{6}$$

where i = 1, 2 refer to the quantities of liquid and air respectively. Both the heated and cold rods are maintained at constant temperature.

In Eqn. (5), Grashof number for liquid is small compared to that of air. This number is defined, in general, for both the liquid and air as

$$Gr^{(i)} = \frac{g \beta^{(i)} z_{(i)}^3 \Delta T}{{\nu^{(i)}}^2} \tag{7}$$

where the value of ΔT is chosen to be equal to temperature difference between the heated and cooled rods and $z_{(i)}$ is the height of the liquid or air column. For liquid, $z_1 = L$ and for air it is assumed to be equal to height of the air column in absence and presence of partition boundaries respectively. Here $\vec{S}$ refers to the source term

which would appear as surface force term in the y-momentum equation for the present configuration of the bridge.

In Eqn. (6), the product of Reynolds number and Prandtl number in the liquid

$$Re^{(1)}\,\mathrm{Pr}^{(1)} = Ma^{(1)} \tag{8}$$

where $Ma^{(1)}$ is the Marangoni number found for the liquid using Eqn. (1) with ρ, ν and α calculated at mean-fluid temperature ($T_{mf} = (T_{\mathrm{hot}} + T_{\mathrm{cold}})/2$) as reported in Table-1.

Table 1: Physical properties of the working fluids at the mean fluid temperature for all the computational conditions (mean fluid temperature remains constant)

$T_{\mathrm{mf}} = 315\mathrm{K},\ T_{\mathrm{amb}} = 300\mathrm{K}$		
	Oil	**Air**
ρ [kg / m^3]	905	1.124
c_p [J / kg.K]	1670	1006
k [W / m.K]	0.14	2.74×10^{-2}
ν [m$^2/s$]	3.64×10^{-6}	1.72×10^{-5}
α [m$^2/s^2$]	9.26×10^{-8}	2.45×10^{-5}
μ [Pa.s]	3.29×10^{-3}	1.8×10^{-5}
β [1 / K]	1.09×10^{-3}	3.17×10^{-3}
σ_{25^oC} [N / m]	1.97e-2	-
σ_T [N / m.K]	-6.37e-5	-
Pr	39.3	0.702
Ma	15670	

The governing equations have been non-dimesnionalized using the dimensionless variables $\bar{r} = r/L$, $\bar{z} = z/L$, $\bar{u} = u/u_{ref}$, $\bar{p} = p/(\rho u_{ref}^2)$ and $\bar{T} = (T - T_{ref})/(T_{hot} - T_{cold})$. Here T_{ref} has been chosen as the ambient temperature T_{amb}. For simplicity of presentation, the over-bar on the non-dimensional variable quantities has been dropped and they have been replaced by respective current variable quantities.

4 Boundary conditions, grid and numerical solution technique

4.1 Boundary conditions for the computational domain

The boundary conditions for the computational domain must be segregated as for the liquid, for the air and the interfacial one. The top surface of the liquid bridge is obviously an isothermal wall type boundary of the heated rod and the bottom

surface is the isothermal wall boundary of the cold rod. For the interface, the temperature boundary conditions have been considered to be Neumann type and so the local temperature values are obtained by solution of the governing equations. The other boundary conditions can be summarized as follows:

Near axis of symmetry :

$(r=0)$; $u_r^{(1)}=0, \partial u_z^{(1)}/\partial r=0, \partial T^{(i)}/\partial r=0$ $(i=1,3)$

Top end of the upper rod $(0<r<1/2AR$, z = *1 + 2H/L*):

$$T=T_{\text{hot}}$$

Bottom end of lower rod $(0<r<1/2AR, z=0)$:

$$T=T_{\text{cold}}$$

Upper and lower surfaces of partition disks $(1/2AR<r<R/L$, z = *(H – Hp)/L* and *(H + Hp)/L*):

$$u_r^{(2)}=0, u_z^{(2)}=0, \partial T^{(2)}/\partial z=0$$

Liquid-air interface:

Velocity: $u_r^{(1)}=u_r^{(2)}=0, \quad u_z^{(1)}=u_z^{(2)}$

Heat flux continuity : $-k^{(1)}\partial T^{(1)}/\partial r=-k^{(2)}\partial T^{(2)}/\partial r$

Shear stress: $\sigma_T\ \partial T^{(1)}/\partial z=-\mu^{(1)}\left(\partial u_z^{(1)}/\partial r\right)+\mu^{(2)}\left(\partial u_z^{(1)}/\partial r\right)$

Side-open boundary $(r=R/L, 0<z<1/2H/L+1)$:

$$p^{(2)}=p_{ref}^{(2)}, \quad \partial T^{(2)}/\partial r=0,\ \partial u_z^{(2)}/\partial r=0,\ u_r^{(2)}=0$$

Top and bottom confined boundaries $(1/2AR<r<R/L$, z = 0 and $2H/L+1)$:

$$p^{(2)}=p_{ref}^{(2)}, \quad \partial T^{(2)}/\partial r=0,\ u_z^{(2)}=0,\ u_r^{(2)}=0$$

Here the side-open boundary is a free shear boundary with impermeable in radial direction and insulated. The top and bottom boundaries are no-slip wall type and insulated. Even though they do not mimic the actual experimental conditions correctly, they are expected to approximately bring in the effect of upper and lower surfaces of the enclosure to the upper and lower boundaries of the computational domain.

The reference pressure has been assumed to be p_{ref} = 101.325 kPa. At the liquid-air interface, the balance between the shear stress in both the liquid and air and surface tension stress has been considered. However, in order to mimic the actual situation of the experimental set up shown in Fig. 1, the top and bottom boundaries are considered to be no-slip wall type with their temperatures maintained at ambient conditions.

4.2 Grid and solution method

The schematic of the axisymmetric grid-mesh used for computations is shown in Fig.3. All the computations have been carried out using a grid size of 90×120 ($\mathrm{N}_r = 90, N_z = 120$). The grid-spacing is sufficiently smaller near the interface compared to far regions inside the liquid as well as air. This is necessary in order to resolve the steep gradients of quantities near the interface.

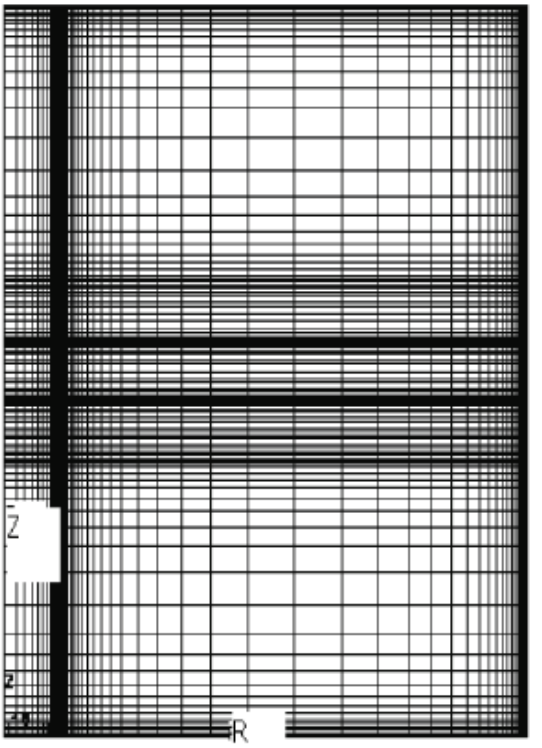

Figure 3: Schematic of the axisymmetric grid-mesh used for computations

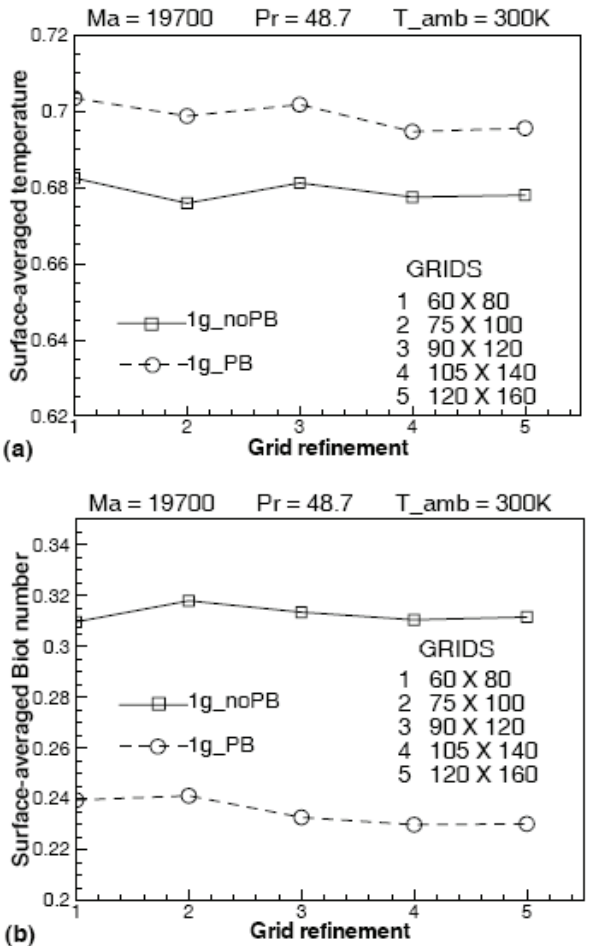

Figure 4: Effect of grid refinement on (a) surface-averaged temperature (b) surface-averaged Biot number for 1g_noPB and 1g_PB (Ma = 15670, T_{amb} = 300K)

The final grid size for all the computations has been chosen after confirming a thorough grid-independence. Figs. 4(a) and (b) present the effect of grid refinement on surface-averaged temperature and surface-averaged Biot number respectively. Any further refinement of the grid beyond 90×120 does not offer significant improvement in the value of surface-averaged temperature as well as surface-averaged Biot number.

The numerical solutions are obtained using commercial CFD software (Star-LT). Since the solver does not handle thermocapillary boundary condition explicitly, the

surface tension is expressed as a body force acting on a very thin layer defined at the surface of the liquid bridge.

$$F_{body} = \sigma_T \frac{\partial T^{(1)}}{\partial z} \frac{1}{\delta r} \tag{9}$$

where δr is the differential thickness of the thin layer on the surface of the liquid-bridge. This body force term appears as an explicitly discretized source term in the solution of z-component of the momentum equation.

The expression of Eqn. (9) follows easily for a very thin elemental liquid volume at the interface of height dz and radial width δr. For a unit thickness (normal to the plane) of the thin elemental liquid layer at the interface, the differential surface tension force acting on the layer becomes

$$d\sigma^{(1)}.1 = \frac{\partial \sigma^{(1)}}{\partial T} \frac{\partial T}{\partial z}.dz.1$$

Hence, the unbalanced force per unit volume of the element, or the body force is obtained by dividing this force by volume of the element (= $dz\,.\delta r\,.1$) as given in Eqn. (9) above. It is to emphasize that the grid spacing near the liquid-air interface must be small enough to avoid any grid dependency in the computation. Consequently, the modeling of surface tension term as a body force term is not a bad assumption if the grid spacing is kept sufficiently small at the liquid-air interface. In fact, even the classical Marangoni force formulation is based on the same differential force concept for a continuum of the fluid element.

5 Validation of computations

Figures 5(a) and (b) present a comparison of radial variation of temperature between computed results and the experimentally measured data at horizontal planes located 0.12 mm and 1.44 mm from the hot rod respectively. The results correspond to Pr = 41.6 and Ma =14690. The values of Ma and Pr have been calculated after taking into account the temperature dependence of fluid properties which are found at mean fluid temperature ($T_{\rm mf} = (T_{\rm hot} + T_{\rm cold})/2$). It is observed from both experimental as well as computed results that radial temperature gradient is steeper near the hot disk. Since at the side open boundary the temperature boundary conditions are of insulation type, i.e. $\partial T^{(2)}/\partial r = 0$, due to steep temperature gradients near the hot disk, in Fig. 5(a), this boundary condition gets satisfied close to the right open boundary. The variation of computed surface temperature (CFD) shows a good agreement with experimental results. The small deviations of computed results from measured data at the edge of computational domain in Fig. 5(a) and

in middle region of Fig. 5(b) is mainly due to surface tension being modeled as body force term in the computations. A more accurate model would show a better agreement.

6 Results and discussion

6.1 Experimental results

The results report the critical temperature (ΔT_{cr}) difference and critical Marangoni number (Ma_{cr}) dependence upon ambient air temperature for different values of the volume ratio (VR) of the liquid bridge. The effect of natural convection in the surrounding air has been suppressed by mounting the partition boundaries. Moreover, the heating of the ambient air is achieved by enclosing the whole liquid bridge set up in an insulated enclosure and control the heat supplied to air with the help of a low velocity hair dryer. For each case of the study, the ambient temperature has been found as an average value of the temperatures recorded at four to five vertical locations little beyond the radial distance from the axis of the liquid bridge equal to outer radius of the partition boundaries. It is assumed that ambient temperature does not show significant variation at other vertical azimuthal locations. Thermocouples are suspended from the ceiling of the enclosure symmetrically around the liquid bridge. Even though in actual experiment, there would be temperature gradient in the air region, the assumption is made for the ease of numerical computations.

Figures 6(a) and (b) present the variation of ΔT_{cr} and Ma_{cr} respectively with ambient air temperature in presence of partition boundary for four different values of volume ratios (VR). As explained previously, due to small variation in mean fluid properties, Ma_{cr} is directly influenced by ΔT_{cr}. The scattered data indicates that with increasing volume ratio, the onset of oscillatory transition occurs for smaller value of ΔT_{cr}. This is expected due to the reason that a liquid bridge with VR > 1.0 will have convex surface and hence influence of convection in the air region will be more dominant. Even though the partition boundaries are present, the suppression of natural convection also influences the free convex surface more than the concave surface of the bridge causing dynamic surface deformation. Consequently, the liquid bridges having VR < 1.0 would be relatively more stable and onset of instability would occur at higher temperature difference or Marangoni number. However, for VR lower than certain smallest value, the liquid bridge would again become unstable resulting into rupture of interface and bridge collapse with increase in temperature difference.

Figure 7(a) shows a comparison of $\Delta T_{cr}$with variation of ambient air temperature for the cases of 1g_noPB and 1g_PB for a volume ratio (VR) of 1.0 and aspect ratio (AR) of 0.5. The presence of PB results into an increase of ΔT_{cr} over a wide

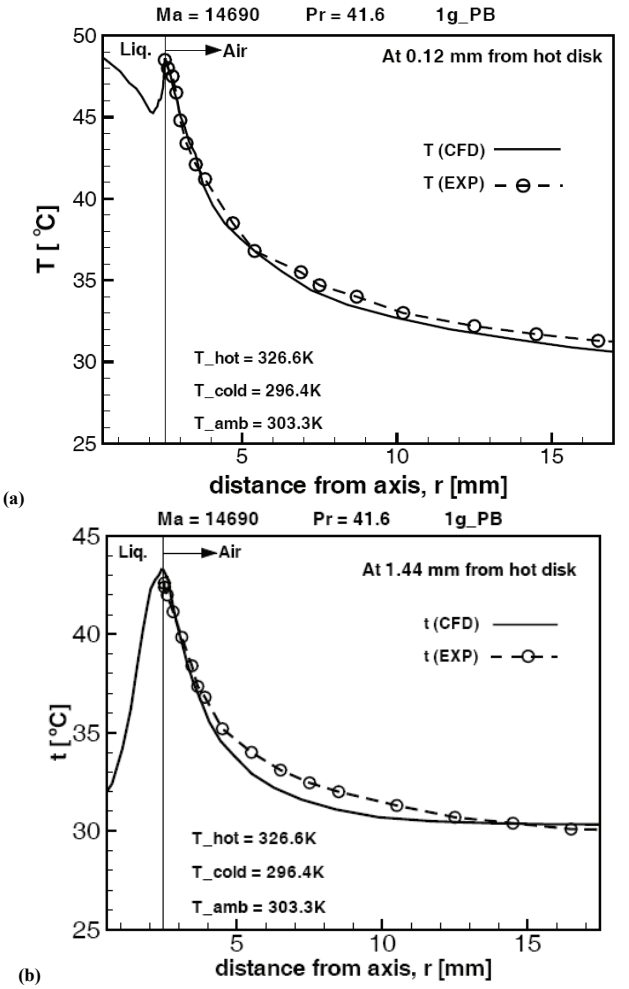

Figure 5: Radial variation of computed temperature distribution compared against experimentally measured values at (a) 0.12 mm (b) 1.44 mm from the hot rod (for Ma = 14690)

range of ambient temperatures considered. Fig. 7(b) presents the variation of Ma_{cr} with ambient air temperature for the above mentioned cases of PB being absent and present for the same values of VR and AR. The values of Ma_{cr} are calculated after considering the temperature dependence of kinematic viscosity in accordance with Eqn. (3) above. However, since the cold and hot rod temperatures have been varied in such a way that the change in mean fluid temperature is less, the effect due to

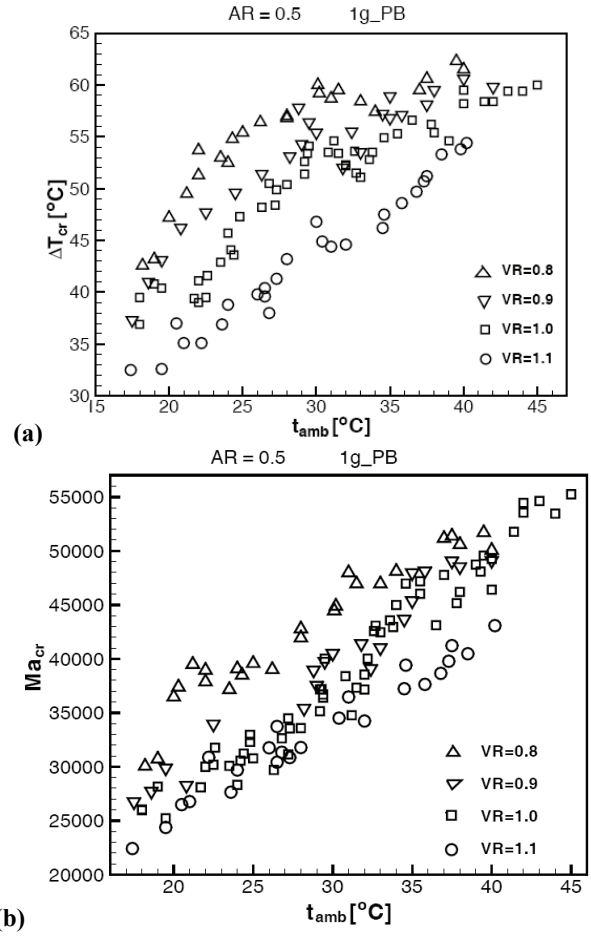

Figure 6: Variation of (a) ΔT_{cr} (b) Ma_{cr} with ambient air temperature (°C) in presence of partition boundary (PB) for four different volume ratios

variation of fluid properties does not control the value of Ma. In other words, the values of ΔT_{cr} and Ma_{cr} would show nearly similar variation with respect to ambient temperature as observed from Figs. 7(a) and (b). The increase in values of ΔT_{cr} in Fig. 7(a) and that of Ma_{cr} in Fig. 7(b) with an increase in the ambient air temperature indicates that for a given state of natural convection in the surrounding air (normal or suppressed), the onset of transition occurs for larger value of ΔT_{cr} at higher value of ambient air temperature. Moreover, for fixed ambient air temperature, the presence of PB in the surrounding air results into increase in value of Ma_{cr} and hence delay in the onset of oscillatory transition. These results are

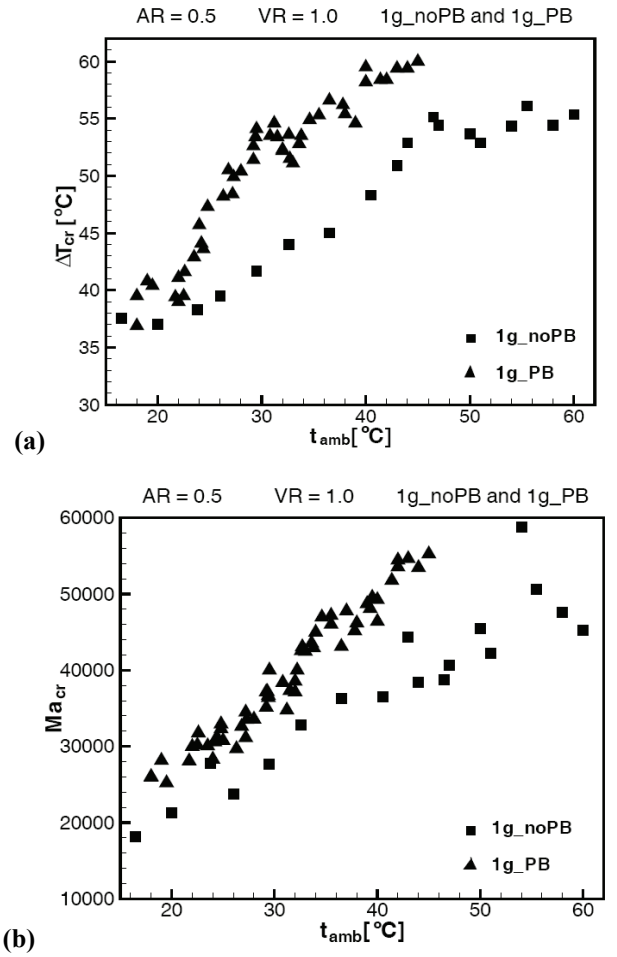

Figure 7: Variation of (a) ΔT_{cr} (b) Ma_{cr} with ambient air temperature (°C) in absence and presence of partition boundary (PB) (VR = 1.0, AR = 0.5)

not in full agreement with those proposed by Wang, Kamotani and Yoda (2007). They observed for thin liquid bridges that initially with an increase in ambient air temperature, ΔT_{cr} increases and after a particular value of the ambient air temperature, ΔT_{cr} decreases abruptly to a much lower value. Their results correspond to aspect ratio, AR = 0.67 and two different heights and diameters, viz. heights of 1.4 mm and 2.0 mm and diameters of 2 mm and 3 mm respectively. However, in the present study the diameter of the bridge is 5.0 mm and height is 2.5mm. Hence, the instability conditions for thicker liquid bridge can be different from those for thin

bridges. It is expected that thinner bridges would have smaller VR_{max} values for stability than the thicker bridges. Accordingly, a direct comparison can be made between different liquid bridges for their stability range only with the help of a reduced parameter.

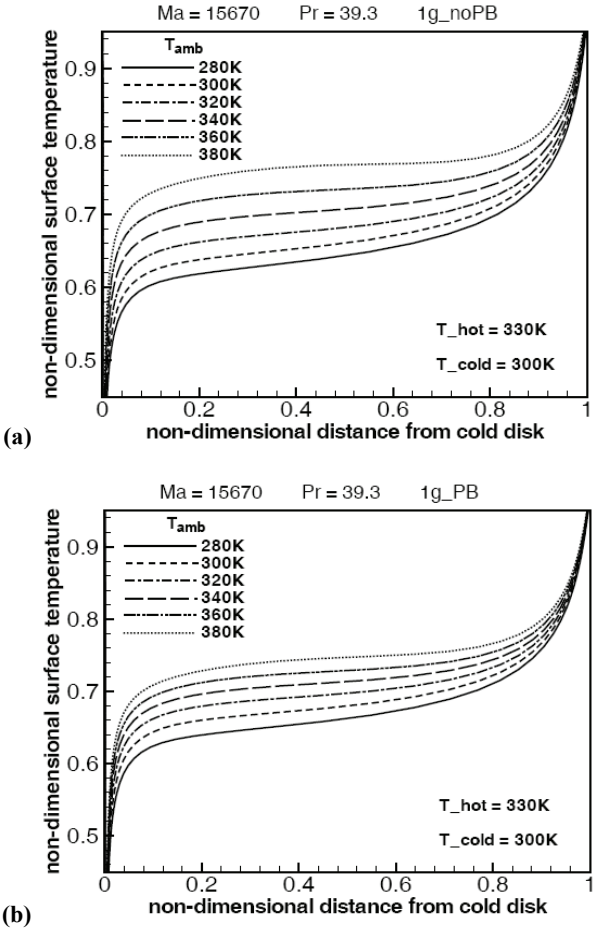

Figure 8: Variation of non-dimensional surface temperature along height of liquid bridge for six different values of ambient temperature under normal gravity in (a) absence (b) presence of PB (Ma = 15670)

6.2 Numerical results

The numerical computations are carried out using CFD software Star-LT for fixed values of hot and cold rod temperatures of T_{hot} = 330 K and T_{cold} = 300K. The

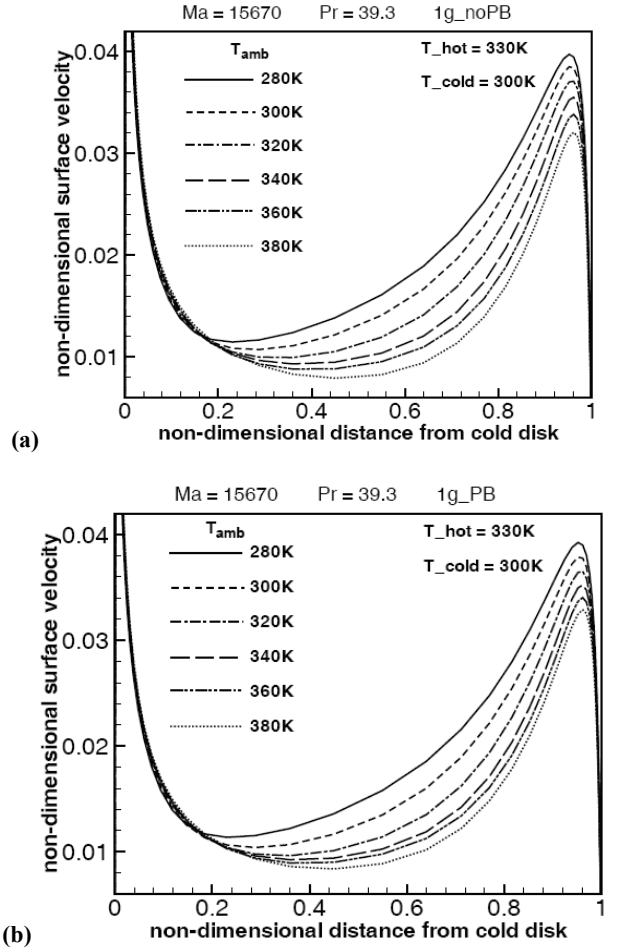

Figure 9: Variation of non-dimensional surface velocity along height of liquid bridge for six different values of ambient temperature under normal gravity in (a) absence of PB (b) presence of PB (Ma = 15670)

fluid properties are interpolated at mean fluid temperature of T_{mf} = 315K. Table-1 summarizes the properties of liquid and air at the mean fluid temperature. Consequently, for all the computational conditions, the Marangoni number and Prandtl number of the liquid are found to be Ma = 15670 and Pr = 39.3.

Figures 8(a) and (b) present the variation of non-dimensional surface temperature at the surface of the liquid bridge along its height for various ambient temperature values in absence and presence of PB for Ma = 15670. The non-dimensional

surface temperature at a particular location is defined as

$$\theta(D/2,z) = \frac{T(D/2,z) - T_{\text{cold}}}{T_{\text{hot}} - T_{\text{cold}}} \tag{10}$$

The surface temperature is observed to increase from cold to the hot rod both in absence and presence of PBs respectively. Moreover, at a given height location on the free surface of the liquid bridge, the temperature is higher for higher value of the ambient temperature due to suppression of natural convection responsible for convective heat transfer across the free surface of the liquid.

At low ambient temperature (T_{amb} < 300K), the local surface temperature of the bridge is smaller in absence of PBs than in their presence. On the other hand, at higher ambient temperature (T_{amb} > 330K), the local surface temperature is higher in absence of PBs. The observation gives a clear indication of more heat transfer from the surface to air or from air to the surface (depending upon the ambient temperature) in absence of PB. Thus, the presence of PB causes reduction in convective heat transfer across the surface.

Figs. 9(a) and (b) present the variation of non-dimensional surface velocity which has been non-dimensionalized with respect to the Marangoni velocity, $u_{ref} = \sigma_T \Delta T / \rho\, \nu$ along height of the liquid bridge for 1g_noPB and 1g_PB respectively. The surface velocity near the cold disk is zero and then it abruptly increases to a larger value from where it keeps on decreasing along height of the liquid bridge. The surface velocity at any height location decreases with increase in ambient temperature. The decrease in surface velocity lowers the value of local convection heat transfer coefficient at a particular location. This results into an increase in the surface temperature at the location. A comparison of Figs. 9(a) and (b) reveals that the influence of change in ambient temperature on local variation of surface velocity is relatively more in presence of PB than in absence of PB. This is mainly due to suppressed natural convection effect in presence of PB.

Figures 10(a) and (b) present the variation of local Biot number (Bi) at the liquid-air interface along height of the liquid bridge for six different ambient temperatures in absence and presence of PB respectively. The local Biot number at a particular height location may be written as

$$Bi_{local}(z) = \frac{q(z)\, L}{k\, \Delta T}, \tag{11}$$

where $q(z)$ is the heat flux across the interface, k is the thermal conductivity of the liquid and ΔT is the temperature difference between the hot and cold rods. A positive value of Bi refers to heat loss from the liquid to air and vice versa. The

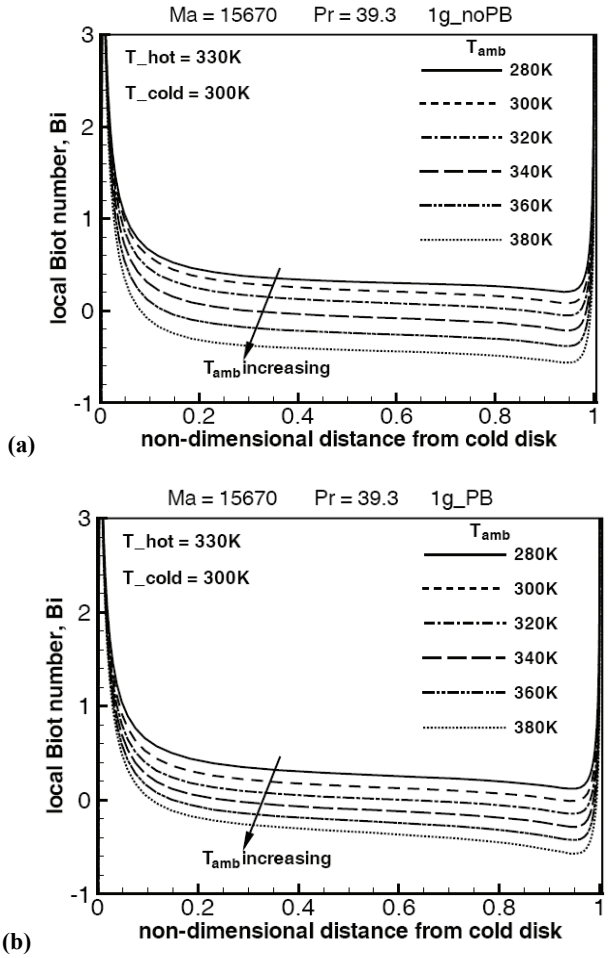

Figure 10: Variation of local Biot number along height of liquid bridge for six different values of ambient temperature under normal gravity in (a) absence (b) presence of partition boundary

average Biot number at the liquid-air interface can be written as

$$Bi_{avg} = \frac{Q_{\text{interface}}\, L}{A\,(k\Delta T)} \tag{12}$$

Here $Q_{interface}$ is the overall heat transfer across the interface and A is the area of the interface.

It is apparent from Figs. 10(a) and (b) that an increase in ambient temperature

causes a decrease in local Biot number at a particular location of the interface. Moreover, beyond certain value of ambient temperature, Bi_{local} becomes negative and the conditions change from heat loss to those of heat gain. At lower values of ambient temperature, the overall heat loss from the interface in presence of PB is less than that in absence of PB while at higher ambient temperature also the heat gain by the interface in presence of PB is less than in absence of PB. This is primarily due to suppression of natural convection effect in presence of PB for both heat loss as well as heat gain situations. On the other hand, the experimental results from Figs. 7(a) and (b) show that onset of oscillatory transition (both in terms of critical temperature difference, ΔT_{cr} as well as critical Marangoni number, Ma_{cr}) gets delayed both due to the effect of suppression of natural convection in the surrounding gas or by ambient heating.

Thus, the results show that heat loss at the liquid-air interface has a destabilizing effect and would result into pre-onset of transition, which refers to onset of instability at lower values of Marangoni number. Under microgravity environment, the natural convection effect gets completely eliminated due to which the only mode by which heat transfer from/to the interface occurs is by radiation. Consequently, the onset of instability induced by free surface deformations gets triggered at higher values of temperature difference across the liquid bridge.

Figures 11(a) and (b) present the variation of surface-averaged Biot number and surface-averaged temperature against the non-dimensional ambient temperature for 1g_noPB and 1g_PB configurations respectively. The ambient temperature has been non-dimensionalized as follows:

$$\theta_{\text{amb}} = \frac{T_{\text{amb}} - T_{\text{mf}}}{T_{\text{hot}} - T_{\text{cold}}} \tag{13}$$

In Fig. 11(a), with an increase in the ambient temperature, the surface-averaged Biot number decreases both in absence and presence of the PB. However, the surface-averaged Biot number in presence of PB is smaller than in its absence and the average Biot number becomes zero at a smaller value of the ambient temperature in presence of the partition boundary. In other words, the conditions in the presence of PB change to those of net surface heat gain at relatively lower value of ambient temperature than in absence of PB. Fig. 11(a) also shows that there exists a value of ambient temperature beyond which even heat gain in presence of PB gets suppressed. The effect of heat loss or heat gain at the free surface of the liquid bridge appears in terms of overall heating or cooling of the liquid-air interface. The heat transfer across the interface results into a change of temperature of the interface. Fig. 11(b) shows the variation of average temperature of the free liquid bridge surface with non-dimensional ambient temperature (θ_{amb}). Below a particular value of the ambient temperature ($\theta_{\text{amb}} < 1.5$ or $T_{amb} < 45^{\circ}$C), the average

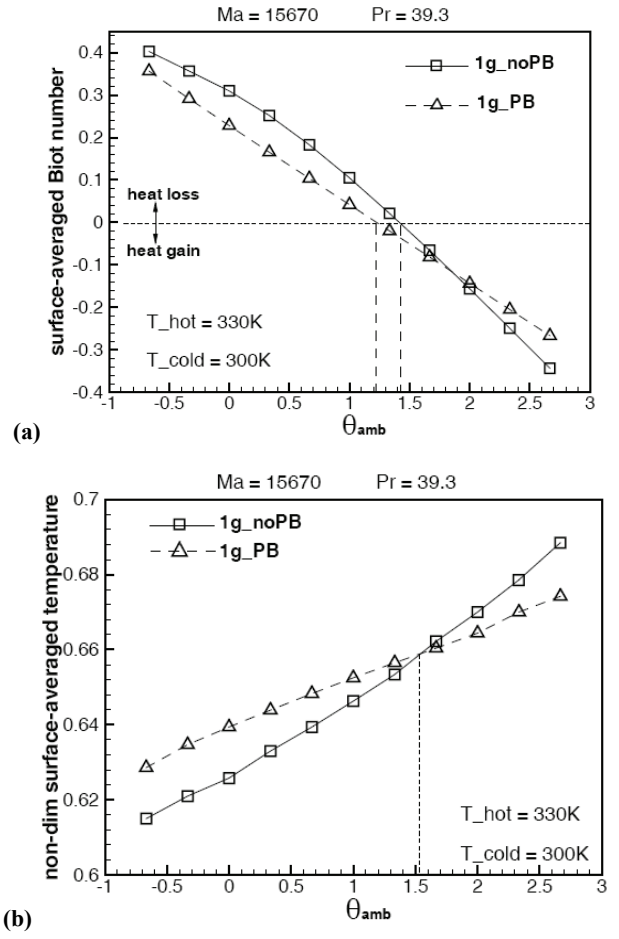

Figure 11: Variation of (a) surface-averaged Biot number (b) surface-averaged temperature, with non-dimensional ambient temperature (with respect to cold rod) for 1g_noPB and 1g_PB (Ma = 15670)

temperature of the interface is smaller in absence of PB which is due to more heat loss from the free surface. However, for $\theta_{\text{amb}} > 1.5$ or $T_{amb} > 45^{\circ}$C, the average surface temperature in presence of PB becomes smaller. This is primarily due to suppression of convection heat transfer responsible for both heat loss as well as heat gain.

7 Conclusions

The present experimental study with accompanied numerical study attempts to relate the effect of suppression of natural convection in the surrounding air to the onset of oscillatory instability in a half-floating-zone liquid bridge of high Pr fluid. Experimental study confirms that the onset of instability gets delayed in presence of PB in the surrounding air for prescribed ambient temperature. Similar effect is observed due to heating of the ambient air in absence as well as presence of PB. The numerical study reports that the presence of PB suppresses the heat loss from the free surface of the liquid. Consequently, it can be inferred that the heat loss across the free surface of the liquid bridge would result into a decrease of the critical Marangoni number (Ma_{cr}) for onset of oscillatory instability. In other words, for the considered value of AR (= 0.5) of the liquid bridge, due to suppression of natural convection in the surrounding air or by reducing the surface heat loss, the value of Ma_{cr} can be increased and onset of instability can be delayed.

Nomenclature

A	area [m^2]
Ar	aspect ratio ($=L/D$)
Bi	local Biot number $(Q/A)L/(k\Delta T)$ at the liquid-air interface ($=\frac{Q_{\text{interface}}\,L}{A\,(k\Delta T)}$)
c_p	specific heat [J/(kg.K)]
D, D_0	Diameter of liquid bridge, diameter of cylindrical gap [m]
F_{body}	body force [$\mathrm{N/m}^3$]
Fr	Froude number = $\left\{u_{ref}^2/L.g\right\}^{0.5}$
Gr	Grashof number ($=g\beta L^3\Delta T/\nu^2$)
g	acceleration due to gravity [$\mathrm{m/s}^2$]
H	height of each cold and hot rod [m]
H_p	height of upper PB from lower surface of upper rod or height of upper surface of lower rod from lower PB
k	thermal conductivity [W/(m.K)]
L	height of the liquid bridge column [m]
Ma	Marangoni number = $Re.Pr$ ($=\frac{\sigma_T \Delta T L}{\rho \nu \alpha}$)
N_r, N_z	Number of grids in radial and axial directions
Pr	Prandtl number ($=\frac{\nu}{\alpha}$)
p	pressure [Pa]
p_{ref}	reference pressure ($=p_{amb}$)
Q	heat flow [W]
R	radius of the computational domain [m]

Re	Reynolds number = $u_{ref}L/\nu$
r, z	radial and axial coordinates
$\vec{S}$	source term
T, T_{ref}	temperature and reference temperature [K]
T_{amb}	ambient temperature [K]
T_{cold}	temperatures of cold rod [K]
T_{hot}	temperature of hot rod [K]
T_{mf}	mean fluid temperature for liquid = (T_{hot} + T_{cold})/2
t	temperature [°C] = $T - 273.15$
t_{amb}	ambient temperature [°C] = $T_{amb} - 273.15$
u_{ref}	reference velocity [m/s] = $\lvert\sigma_T\rvert \Delta T/\mu$
V, V_0	volume of liquid and volume of gap [m^3]

Greek

α	thermal diffusivity [m^2/s]
β	volume coefficient of expansion [1/K]
ΔT	temperature difference = $T_{hot} - T_{cold}$ [K or °C]
μ	dynamic viscosity [Pa.s]
ν	kinematic viscosity [m^2/s]
θ_{amb}	non-dimensional temperature
ρ	density [kg/m^3]
σ	surface tension [N/m]
σ_T	temperature coefficient of surface tension [N/(m.K)]

Notations

1g_noPB	PB absent under gravity
1g_PB	PB present under gravity
HFZ	half-floating-zone
TC	thermocapillary convection
VR	volume ratio (=V/V_0)

References

Chun, C. H.; Wuest, W. (1978): A microgravity simulation of the Marangoni convection. *Acta Astronautica*, vol. 5, No. 9, pp. 681.

Chun, C. H.; Wuest, W. (1979): Experiments on surface tension driven flow in floating zone melting. *Acta Astronautica*, vol. 6, pp. 1073.

Chun, C. H.; Wuest, W. (1981): Correlations of oscillations of flow and temperature in floating-zone under microgravity. *Adv. Space Res.*, vol. 1, No. 5, pp. 17.

Chun, C. H. (1980): Experiments on steady and oscillatory temperature distribution in a floating zone due to the Marangoni convection. *Acta Astronautica*, vol. 7, pp. 479.

Gelfgat, A.Yu.; Rubinov, A.; Bar-Yoseph, P.Z.; Solan, A. (2005): On the three-dimensional instability of thermocapillary convection in a arbitrarily heated floating zones in microgravity environment. *FDMP: Fluid Dynamics and Mat. Processing*, vol. 1, pp. 21.

Imaishi, N.; Yasuhiro S.; Akiyama, Y.; Yoda, S. (2001): Numerical simulation of oscillatory Marangoni flow in half-zone liquid bridge of low Prandtl number, *J. Cryst. Growth*, vol. **230**, pp. 164.

Kamotani, Y.; Ostrach, S. (1998): Theoretical analysis of thermocapillary flow in cylindrical columns of high Prandtl number fluids. *ASME J. Heat Transfer*, vol. 120, pp. 758.

Kamotani, Y.; Ostrach, S.; Vargas, M. (1984): Oscillatory thermocapillary convection in a simulated floating-zone configuration. *J. Cryst. Growth*, vol. 66, pp. 83.

Kamotani, Y.; Wang, L.; Hatta, L.; Wang, A.;Yoda, S. (2003): Free surface heat loss effect on oscillatory thermocapillary flow in liquid bridges of high Prandtl number fluid. *Int. J. of Heat and Mass Transfer*, vol. 46, pp. 3211.

Kobayashi, N. (1984): Computer simulation of the steady flow in a cylindrical floating zone under low gravity. *J. Cryst. Growth*, vol. 66, pp. 63.

Lai, C. L. (2004): Multiple-scale analysis of oscillatory thermocapillary convection of high Prandtl number fluids in a rectangular cavity. *Int. J. Heat Mass Transfer*, vol. 47, pp.1069.

Leypoldt, J.; Kuhlmann, H.C.; Rath, H.J. (2000): Three-dimensional numerical simulation of thermocapillary flows in cylindrical liquid bridges. *J. Fluid. Mech.*, vol. 414, pp. 285.

Masud, J.; Kamotani Y.; Ostrach, S. (1997): Oscillatory thermocapillary flow in cylindrical columns of high Prandtl number fluids. *J. Thermophys. Heat Transfer*, vol. 11, pp.105.

Monti, R.; Albanese, C.; Cartenuto, L.; Castagnolo, D.; Evangelista, G. (1995): An investigation on the onset of oscillatory Marangoni flow. *Adv. Space Res.*, vol.

16, No. 7, pp. 87.

Nishino Koichi; Tiwari Shaligram (2007): Effect of heat loss on Marangoni convection in a liquid bridge. *J. Jpn. Soc. Microgravity Appl.*, vol. 24, pp. 54.

Ostrach, S. (1979): Low-Gravity Fluid Flows. *Annu. Rev. Fluid Mech.*, vol. 14, pp. 313.

Ostrach, S.; Kamotani, Y., Lee, J. (1993): Osciollatory thermocapillary flows. *Adv. Space Res.*, vol. 13, No. 7, pp. 97.

Pimputkar, S.M.; and Ostrach, S. (1980): Transient thermocapillary flow in thin layers. *Phys. Fluids*, vol. 23, pp. 1281.

Schwabe, D.; Scharmann A.; Preisser, R. (1981): Verification of the oscillatory state of thermocapillary convection in a floating zone under low gravity, *Acta Astronaut.*, vol. 9, pp. 265.

Schwabe, D.; Scharmann, A.; Preisser, F.; Oeder, R. (1978): Experiments on surface tension driven flow in floating zone melting. *J. of Crystal Growth*, vol. 43**,** pp. 305.

Shevtsova, V.M.; Mialdun, A.; Mohamed, M. (2005): A study of heat transfer in liquid bridges near onset of instability. *J. Non-Equilib. Thermodyn.*, vol. 30, No. 3, pp. 261.

Shevtsova, V. M.; Melnikov, D.E.; Legros, J.C. (2001): Three-dimensional simulations of hydrodynamic instability in liquid bridges. Influence of temperature dependent viscosity. *Physics Fluids*, vol. 13, pp. 2851.

Shevtsova, V. M.; Melnikov, D.E.; Legros, J.C. (2004): Change of flow patterns in thermocapillary convection in liquid bridges. *Acta Astronautica*, vol. 54, pp. 493.

Shin-Etsu Chemicals Co. Ltd. (1991): Silicone oil KF96. Technical note (in Japanese).

Smith, M. K; Davis, S. H. (1983): Instabilities of dynamic thermocapillary liquid layers. Part 1. Convective instabilities. *J. Fluid Mech.*, vol. 132, pp. 119.

Tiwari Shaligram; Nishino Koichi (2007): Numerical study to investigate the effect of partition block and ambient air temperature on interfacial heat transfer in liquid bridges of high Prandtl number fluid. *J. Cryst. Growth*, vol. 300, pp. 486.

Ueno, I.; Tanaka, S.; Kawamura, H. (1991): Oscillatory and chaotic thermocapillary convection in a half-zone liquid bridge. *Phys. Fluids*, vol.15, pp. 408.

Velten, R.; Schwabe, D.; Scharmann, A. (1991): The periodic instability of thermocapillary convection in cylindrical liquid bridges. *Physics Fluids A*, vol.3, pp. 267.

Wanschura, M.; Shevtsova, V. M.; Kuhlmann, H. C.; Rath, H. J. (1995): Convective instability mechanisms in thermocapillary liquid bridges. *Phys. Fluids*, vol.7, pp. 912.

Wang, A.; Kamotani, Y.; Yoda, S. (2007): Oscillatory thermocapillary flow in liquid bridges of high Pr fluid with free surface heat gain. *Int. J. Heat Mass Transfer*, vol.50, pp. 4195.